BB

GSI

Preprint 2000 - 05
Februar

ISOTOPIC PRODUCTION CROSS SECTIONS OF FISSION RESIDUES IN ^{197}Au-ON-PROTON COLLISIONS AT 800 A MeV

J. Benlliure, P. Armbruster, M. Bernas, A. Boudard, J.P. Dufour, T. Enqvist, R. Legrain, S. Leray, B. Mustapha, F. Rejmund, K.-H. Schmidt, C. Stephan, L. Tassan-Got, C. Volant

(Submitted to Nucl. Phys. A)

Gesellschaft für Schwerionenforschung mbH
Planckstraße 1 • D-64291 Darmstadt • Germany
Postfach 11 05 52 • D-64220 Darmstadt • Germany

Isotopic production cross sections of fission residues in ^{197}Au-on-proton collisions at 800 A MeV

J. Benlliure [a,b], P. Armbruster [b], M. Bernas [c], A. Boudard [d], J.P. Dufour [e], T. Enqvist [b], R. Legrain [d], S. Leray [d], B. Mustapha [c], F. Rejmund [c], K.-H. Schmidt [b], C. Stéphan [c], L. Tassan-Got [c], C. Volant [c]

[a] *Universidad de Santiago de Compostela, 15706 Santiago de Compostela, Spain*

[b] *Gesellschaft für Schwerionenforschung, Planckstr. 1, 64291 Darmstadt, Germany*

[c] *Institut de Physique Nucléaire, 91406 Orsay Cedex, France*

[d] *DAPNIA/SPhN, CEA/Saclay, 91191 Gif sur Yvette Cedex, France*

[e] *CENBG, 33175 Gradignan Cedex, France*

Interactions of ^{197}Au projectiles at 800 A MeV with protons leading to fission are investigated. We measured the production cross sections and velocities of all fission residues which are fully identified in atomic and mass number by using the in-flight separator FRS at GSI. The new data are compared with partial measurements of the characteristics of fission in similar reactions. Both the production cross sections and the recoil energies are relevant for a better understanding of spallation reactions.

Key words: Spallation reactions; Fission residues; p(^{197}Au,X), E=800 A MeV; Isotopic identification; Kinetic energies.
PACS: 25.40.Sc, 25.85.Ge, 24.75.+i, 27.50.+e, 27.60.+j

1 Introduction

Recently, spallation reactions have gained new interest because they can be used as neutron sources for many applications in material-science investigations [1] or in nuclear-waste transmutation [2]. They are also important for their implications in the production of radioactive nuclear beams (RNB) [3] or in nuclear astrophysics [4]. A common point to all these applications is the production of heavy residues, the precise knowledge of which will help to determine the nuclear species that can be used as RNB, to understand the

observed composition of cosmic rays or the radioactive pollution and material damages in spallation neutron sources.

Although lead is considered as the optimum material for a spallation source, gold has been used as a benchmark case for comparing experimental data and model calculations [5]. In addition, gold is close to mercury which has also been proposed to be used in spallation sources.

While in another work we discuss the production of spallation-evaporation residues [6], here we will concentrate on the characterization of the fission fragments. A detailed discussion of the reaction mechanism leading to the production of these residues will be given in a forthcoming publication [7].

The observables that we propose for investigating fission induced in spallation reactions are the isotopic distribution and the kinematical properties of the reaction residues. A few production yields were obtained previously by using gamma-spectroscopic methods [8,9]. The main limitation of this technique is that neither short-lived nor stable residual nuclei can be measured. Other experiments were based on the identification of fission residues with time-of-flight spectrometers [10,11], where only the mass of the residues was measured, or with energy-loss and velocity measurements [12], where only the atomic number of the residues was determined.

The experimental technique used in this work allows to identify all the reaction products in mass number A and atomic number Z by means of a magnetic in-flight separation in inverse kinematics. This technique has already successfully been used to investigate the isotopic production cross sections of fission residues in heavy-ion reactions [13–16] with the FRagment Separator at GSI. Moreover, it has been shown that this is a suitable technique for producing medium-mass neutron-rich isotopes from the fission of ^{238}U [17].

2 Experiment and data analysis.

2.1 Experimental set up

The heavy-ion synchrotron SIS at GSI was used to accelerate ^{197}Au ions up to an energy of 800 A MeV. The beam intensity of typically 10^7 ions/s was continuously measured during the experiment with a secondary-electron monitor (SEETRAM). The beam impinged on a liquid H_2 target of 87.3 mg/cm^2 thickness located at the entrance of the projectile-fragment separator (FRS). In order to subtract the contribution due to nuclear reactions in the windows of the target, an additional dummy target was used, simulating the material

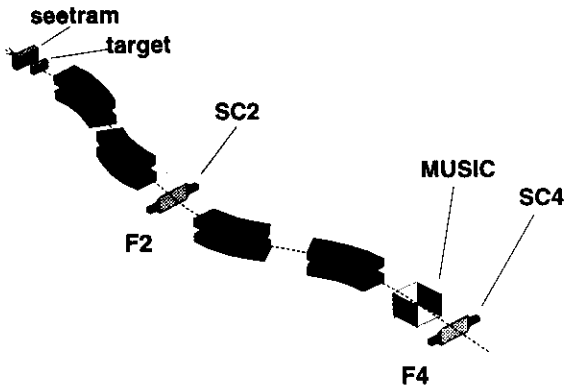

Fig. 1. *Schematic view of the FRagment Separator with its standard detection set-up.*

and thickness of the windows (Ti 36 mg/cm^2).

The reaction residues produced in these collisions were identified in mass and atomic number using the FRagment Separator (FRS) at GSI. This is a zero-degree spectrometer with two symmetric stages in order to ensure the achromatism of the system [18], as shown in figure 1.

2.2 Isotopic identification

The atomic number of the transmitted ions was identified from the energy-loss measurement in a multi-sample ionization chamber (MUSIC) [19]. The recorded values of the energy loss were corrected for velocity and position dependencies. The absolute charge calibration was obtained from different tunings of the FRS in which reaction products from the primary beam down to the fission region were transmitted.

The mass identification was obtained from the magnetic rigidity and time-of-flight of the ions considered. The magnetic rigidity was determined from the transversal positions of the trajectories of the ions at the intermediate and final image planes of the spectrometer. Two position-sensitive plastic scintillators (SC2 and SC4) [20] placed at both image planes (F2 and F4) provided both the positions of the ions and their time-of-flight. Additional multi-wire detectors were used at both image planes to calibrate the position response of the plastic scintillators as well as the drift-time signals from the four anodes of the MUSIC detector. The positions obtained from the different drift-time signals of the MUSIC were used to account for the dependence of the flight path on the horizontal angle of the transmitted ions. This correction is crucial in the case of fission residues because of their large angular range. The final mass values were obtained from the absolute calibration of the time-of-flight. This calibration was determined by slowing down the primary beam by different layers of matter at the intermediate image plane. The mass identification

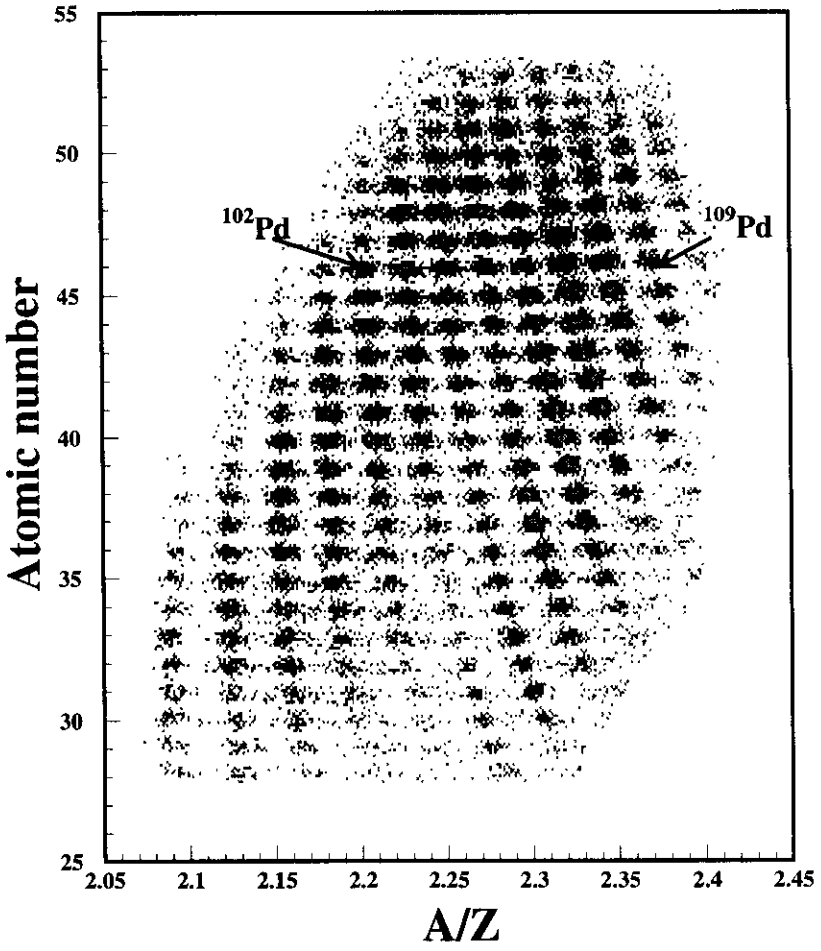

Fig. 2. *Z-A/Z scatter plot of fission residues observed in a typical tuning of the fragment separator for the reaction ^{197}Au (800 A MeV) + p corresponding to a magnetic rigidity of 0.9175 times the magnetic rigidity of the primary beam.*

was cross checked with the one obtained in our measurements with the degrader technique for spallation-evaporation residues [6], where the different isotopes can easily be identified from their positions at both image planes of the spectrometer.

In Fig. 2, we show an example of the mass and charge resolution obtained in a tuning of the FRS corresponding to a magnetic rigidity of $0.9175(B\rho)_o$ where $(B\rho)_o$ is the magnetic rigidity of the beam. The final charge and mass resolution achieved in our measurements for residues produced in fission reactions is $\Delta Z/Z \approx 7 \cdot 10^{-3}$ and $\Delta A/A \approx 2 \cdot 10^{-3}$ (FWHM), respectively.

The first stage of the FRS produces a selection of the transmitted ions in A/q (mass number divided by the ionic charge), while the second one selects the

ions according to their atomic number Z [21]. This selection together with the limited acceptance of the spectrometer ($\Delta B\rho/B\rho \approx 3\%$) determines the isotopes transmitted in one tuning of the spectrometer. In order to cover the full range in magnetic rigidity of about 12%, populated by the fission fragments, with a good overlap, 7 different tunings of the magnetic field B_1 of the first section of the FRS were required. The energy loss of the transmitted ions at the intermediate image plane (vacuum windows, air and plastic scintillator) limited the range of transmitted elements to 20. Therefore, two tunings of the field B_2 of the second stage of the FRS per value of B_1 were needed in order to cover the full range of the fission fragments from Z$\approx$ 20 to Z$\approx$ 60.

3 Production cross sections of fission residues.

3.1 Identification of fission residues.

Reaction residues produced by fission were identified from their kinematical properties. While spallation-evaporation residues have velocities close to that of the beam, the velocity vectors of fission products populate a narrow shell of a large sphere in the frame moving with beam velocity. The radius of this sphere is determined by the Coulomb repulsion between both fission fragments. After conversion into the laboratory frame, the velocity distribution of the fission residues populates the surface of an ellipsoid [13], while spallation-evaporation reactions populate the center of this ellipsoid [15].

Due to the limited acceptance in angle ($\Delta\theta \approx 15$ mr) and momentum ($\Delta B\rho/B\rho \approx 3$ %) of the spectrometer, the momentum distribution of each isotope produced by fission was only partially transmitted in one tuning. Combining different tunings of the FRS, we were able to reconstruct the full momentum distribution within the limits of the angular acceptance. Due to this restricted angular acceptance, only the fission fragments emitted in forward or backward direction were transmitted as discussed in Ref. [13].

The open histogram in figure 3 represents the reconstructed velocity distribution of ^{90}Zr in the frame defined by the velocity of the projectiles in the middle of the target. The angular cut of the spectrometer produces a triple-humped velocity distribution where the central hump corresponds to spallation-evaporation residues and the two others to forward (positive velocities) and backward (negative velocities) emitted fission residues. Therefore, this particular angular cut of the spectrometer allows for a clear identification of the fission residues. Using this technique, 353 different isotopes produced in fission reactions were fully identified in mass and atomic number.

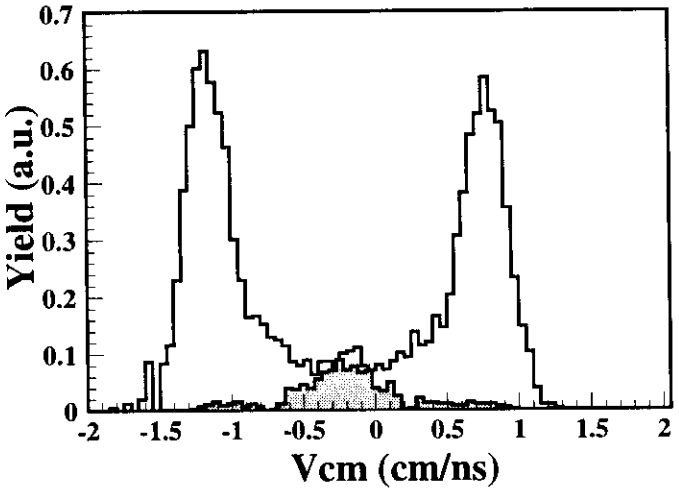

Fig. 3. *Velocity distribution of ^{90}Zr ions in the frame defined by the velocity of the projectiles in the middle of the target obtained with the liquid H_2 target including the titanium windows (open histogram) and with the dummy target (full histogram).*

3.2 Fission yields.

In order to determine the primary fission yields $Y^c(A,Z)$ produced in the reaction, different corrections must be applied. These corrections are mainly determined by the experimental technique and the instrumentation used. They should take into account the losses due to the transmission through the spectrometer (f_{tr}), secondary reactions in the target (f_{tsec}) and in any other layer of matter inside the FRS (f_{sec}), ionic charge states of the measured isotopes (f_q), dead time of the data acquisition (f_τ), and the efficiency of the detectors (f_ε).The primary production yields can be estimated from the measured ones $Y^m(A,Z)$ according to the following expression:

$$Y^c(A,Z) = Y^m(A,Z) \cdot f_{tr} \cdot f_{sec} \cdot f_{tsec} \cdot f_q \cdot f_\tau \cdot f_\varepsilon \qquad (1)$$

In the following sections we will discuss these corrections in detail.

3.2.1 Evaluation of the angular transmission.

The angular transmission of the fission products in the spectrometer is one of the main corrections to be applied to the measured yields in order to determine the final production cross sections. The transmission of any isotope by a magnetic spectrometer is defined by two factors: the kinematics of the considered particle which determines its trajectory inside the spectrometer, and the

momentum and angular acceptances of the apparatus which give the physical constraints to the trajectory of the particle. As already pointed out, the measured yields are only biased by the angular acceptance of the spectrometer because we reconstruct the part of the momentum distribution within the limits of the angular acceptance by using different tunings of the spectrometer.

Standard ion-optical calculations [22,23] are too time consuming to evaluate the transmission of hundreds of different isotopes. Therefore, we used a new approach based on the decoupled description of the kinematics and the angular acceptance of the spectrometer. A detailed description of the method will be published separately [24]. The method uses a parameterization of the angular acceptance of the spectrometer for any possible trajectory followed by the ions, while the kinematics is determined from experiment.

We characterize the trajectory of any ion through the spectrometer by its positions (x_2, x_4) at both image planes. Using standard ion-optical calculations we construct a map of the angular acceptance $\alpha_{lab}(x_2, x_4)$ of the spectrometer as a function of the different possible positions of the ions at the two image planes. This map is determined by the characteristics of the apparatus, it will be valid for any reaction studied.

The transformation of the acceptance angle (α_{lab}) into the center-of-mass frame of the fission fragments will provide two limiting emission angles (α^f_{cm} and α^b_{cm}) which define the transmission in forward and backward direction. The values of the angular transmission can then be obtained by integrating the parts of the angular range populated by fission up to the limiting angles according to the following expressions.

$$T_f = \frac{\int_0^{2\pi}\int_0^{\alpha^f_{cm}(x_2,x_4)} sin\theta d\theta d\phi}{4\pi} = \cdots = \frac{1 - cos\alpha^f_{cm}(x_2, x_4)}{2} \tag{2}$$

$$T_b = \frac{\int_0^{2\pi}\int_{\alpha^b_{cm}(x_2,x_4)}^{\pi} sin\theta d\theta d\phi}{4\pi} = \cdots = \frac{1 + cos\alpha^b_{cm}(x_2, x_4)}{2} \tag{3}$$

The measured longitudinal projections of the forward and backward velocities are used to transform the angular acceptance from the laboratory to the center-of-mass frame. An iterative procedure is applied, because the measured longitudinal projection of the velocity is biased by the angular acceptance.

Using the acceptance map, characteristic of the spectrometer, and applying equations 1 and 2 with the measured positions of each ion at both image planes of the spectrometer and their kinematical properties we can directly determine the transmission of each isotope without any further Monte-Carlo calculation.

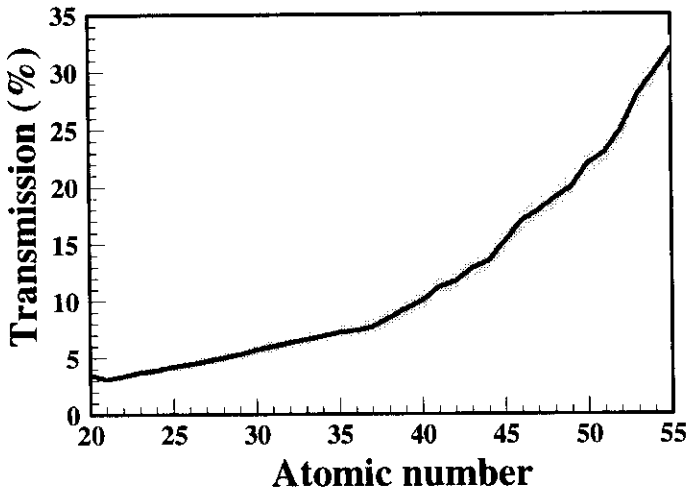

Fig. 4. *Evaluated transmission of the backward-emitted fission residues through the FRS in the reaction ^{197}Au (800 A MeV) + p, as a function of the atomic number. The gray area accounts for the different transmission values of the isotopes of an element given.*

Unfortunately, the momentum distribution of fission residues was not fully covered for all of them emitted in forward direction because their magnetic rigidities partly overlap with the primary beam. Therefore, only the backward-emitted fragments were used to determine the production yields under the assumption that fission is an isotropic process. In figure 4, we represent the calculated transmission of backward-emitted fission residues produced in the considered reaction as a function of the atomic number. The correlation between the mass and the velocity of the fission residues produced by momentum conservation in the fission process explains the observed evolution of the transmission with the atomic number. The small values of the transmission, especially for the lighter isotopes, justify the efforts needed to obtain a reliable evaluation of this correction. As we will see in section 4.1, the agreement between our data and other values found in literature proves the validity of the procedure used to evaluate the transmission. The error associated to this procedure depends on the accuracy of the angular-acceptance values of the spectrometer and the accuracy of the measured velocities of the different isotopes. The estimated error of the angular acceptance is around 4% while the one due to the velocity of the residues is around 12%. The global accuracy of the transmission correction amounts to 13%.

3.2.2 Parasitic reactions.

Additional corrections like the ones due to secondary reactions in the different layers of matter inside the spectrometer or in the target, and reactions in the titanium windows of the liquid hydrogen target must be considered in order

to determine the primary production yields.

The residues of secondary reactions produced in the vacuum windows, the air and plastic scintillator at the intermediate image plane were suppressed by the second stage of the FRS. Therefore, the measured yields were corrected for the losses evaluated from the total interaction cross sections calculated with the formula of Benesh et al. [25]. This correction ranges from 8% for the lightest masses (A≈40) till 17% for the heaviest (A≈130) as can be seen in Fig. 5 (solid line).

A different technique was applied to evaluate secondary reactions in the target. These reactions depopulate the heavier isotopes while they populate the lighter ones. We will assume that the measured residues can only be produced by multiple reactions where fission is the primary process and fragmentation is the secondary process. This is justified if we consider that fission barriers increase dramatically when decreasing the fissility, and then the probability of fission as a secondary process is negligible.

Using these assumptions, we can determine the true production cross section $\sigma_o^{fis}(A,Z)$ of any isotope due to fission by considering that the measured apparent cross section $\sigma_{app}^{fis}(A,Z)$ contains events from heavier fission products which underwent a secondary spallation reaction while there is a depopulation into lighter nuclei. Assuming that these processes depend only on the mass of the nucleus, the true production cross section will be obtained from the following equation:

$$\sigma_o^{fis}(A,Z) = \sigma_{app}^{fis}(A,Z) \cdot f_{tsec}(A) \tag{4}$$

In this case, the effect on the mass distribution is described by the same function f_{tsec}(A):

$$\sigma_o^{fis}(A) = \sigma_{app}^{fis}(A) \cdot f_{tsec}(A) \tag{5}$$

with $\sigma^{fis}(A) = \sum_Z \sigma^{fis}(A,Z)$.

The full problem can be expressed by the following implicit equation:

$$\sigma_o^{fis}(A) = \sigma_{app}^{fis}(A) + \sigma_o^{fis}(A)\sigma_{tot}(A)\frac{N_t}{2} - \sum_{A_i=A+1}^{A_{max}^{fis}} \sigma_o^{fis}(A_i)\sigma_o^{spa}(A_i \longrightarrow A)\frac{N_t}{2} \tag{6}$$

where A_{max}^{fis} corresponds to the mass number of the heaviest isotope produced by fission, $\sigma_o^{spa}(A_i \longrightarrow A)N_t/2$ describes the probability to produce isobars with mass A from a primary fission product of mass A_i, N_t denotes the number of target atoms per area, and $\sigma_{tot}(A)$ is the total interaction cross section. By further assuming that, for a given mass loss $\Delta A = A_i - A$, the value of $\sigma_o^{spa}(A_i \longrightarrow A)$ scales with the total spallation cross section of the primary nucleus $\sigma_{tot}(A_i)$:

$$\frac{\sigma_o^{spa}(A_1 \longrightarrow A_1 - \Delta A)}{\sigma_o^{spa}(A_2 \longrightarrow A_2 - \Delta A)} = \frac{\sigma_{tot}(A_1)}{\sigma_{tot}(A_2)} \tag{7}$$

we estimate the cross section of the spallation process following fission from the isobaric spallation production cross section $\sigma_o^{spa}(A_{pro} \longrightarrow A_{pro} - \Delta A)$ measured for the same reaction [6] and the total interaction cross sections $\sigma_{tot}(A)$ with H_2 obtained from the formula of Kox et al. [26]:

$$\sigma_o^{spa}(A_i \longrightarrow A_i - \Delta A) = \sigma_o^{spa}(A_{pro} \longrightarrow A_{pro} - \Delta A)\frac{\sigma_{tot}(A_i)}{\sigma_{tot}(A_{pro})} \tag{8}$$

The result of this procedure is shown in Fig. 5 (dashed line). As can be seen, the secondary reactions in the target depopulate the heavier fission residues, populating the lighter ones. The absolute value of this correction is lower than 8% over the full range of fission fragments.

In addition, the primary beam is attenuated along the target due to the nuclear interactions. This effect will be considered in the next section.

Finally, secondary reactions in the titanium windows of the target should also be considered. In principle, since the reaction rate in the titanium is only 2% of the one in the hydrogen while the total fission cross section in the reaction of ^{197}Au at 800 A MeV with both materials is similar, we expect only a small contribution due to fission events in the titanium windows. Nevertheless, the production yields of fission residues in the windows were measured by using an additional titanium target with a thickness equivalent to the one of the

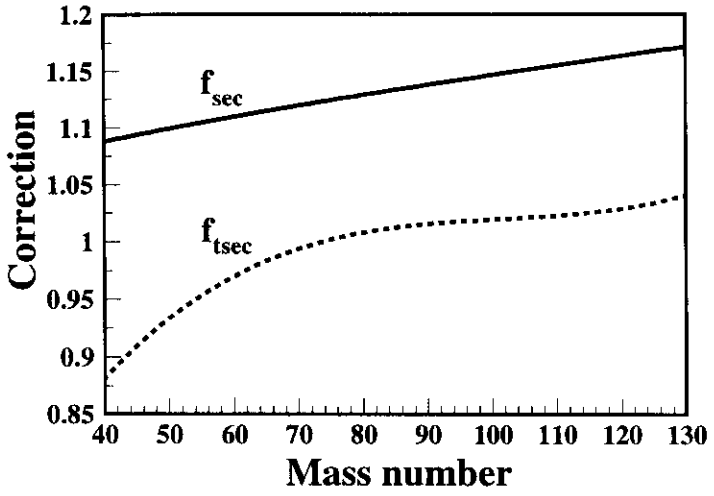

Fig. 5. *Values of the corrections due to secondary reactions applied to the measured yields. The solid line corresponds to the secondary reactions in all the layers of matter inside the FRS behind the target (f_{sec}) while the dashed line represents the correction due to secondary reactions inside the target (f_{tsec}).*

the windows in the hydrogen target (36 mg/cm^2). An example of the obtained results is shown in Fig. 3. In this figure, we compare the measured production yield of ^{90}Zr in the full hydrogen target (open histogram) with the one obtained with the titanium target (gray histogram). As expected, the contribution of fission events is very small. Similar results are obtained for all the produced fission residues. From the data obtained with the two targets, we also conclude that all fragmentation products in the mass range covered by fission are due to reactions in the windows.

3.2.3 Additional corrections.

To determine the primary production cross sections we should account for further corrections as the losses due to ionic charge states of the measured isotopes, the dead time induced by the data acquisition and the detector efficiencies.

The fraction of not completely bare fission residues transmitted through the FRS was estimated by using the procedure described in Ref. [27]. According to these calculations, the fraction of not fully stripped ions is lower than 1% for the full range of elements covered by fission.

The dead time of the data acquisition was measured and registered continuously during the full experiment and in any case was kept below 30%. The final counting rate corresponding to this dead time was of the order of 2000 events per second. The estimated efficiency of the detectors with this typical

counting rates was of the order of 98%.

3.3 Production cross sections.

The final production cross section can be obtained from the corrected isotopic yields $Y^c(A,Z)$, the number of target atoms per area N_t and the number of incident projectiles N_p^* according to the following expression:

$$\sigma(A,Z) = \frac{Y^c(A,Z)}{N_t \cdot N_p^*} \tag{9}$$

The number of target atoms is given by its thickness, which was measured to be (87.3 $\pm$ 2.2) mg/cm^2 [6].

The number of incoming projectiles N_p was determined by using a secondary-electron monitor (SEETRAM) during the full experiment. The signals registered with this monitor were calibrated by using an additional ionization chamber as described in Ref. [28]. The accuracy of this calibration is estimated to be around 6%. The final number of incoming projectiles was corrected by the attenuation of the beam in the target $N_p^* = f_{at} \cdot N_p \quad (f_{at} = 1.06)$.

The measured isotopic production cross sections for all the nuclei identified as being produced in fission are shown in figures 6 and 7. As can be seen, the fission induced by protons on ^{197}Au at 800 A MeV populates a large range of elements from cesium down to argon, and for each element long isotopic chains are produced.

The error bars in figures 6 and 7 correspond to the statistical error. An upper estimate of the statistical uncertainty was deduced from the deviations of the measured cross sections from an assumed smooth behavior of the cross sections. This systematic behavior was obtained from a fit of the measured cross sections as a function of Z for constant N-Z where a smooth evolution of the cross section was observed. The error of each individual isotope was obtained from the rms deviations between the fitted values and the measured ones for some isotopes around the considered isotope. In addition, the systematic errors due to all the corrections applied to the measured yields, the thickness of the target and the primary-beam intensity were estimated to amount to 15%.

The total fission cross section is obtained by summing the partial production cross sections of all isotopes, divided by two, in order to account for the two residues produced in each fission process. Following this procedure, the total fission cross section amounts to σ_f^{tot} = (65$\pm$10) mb.

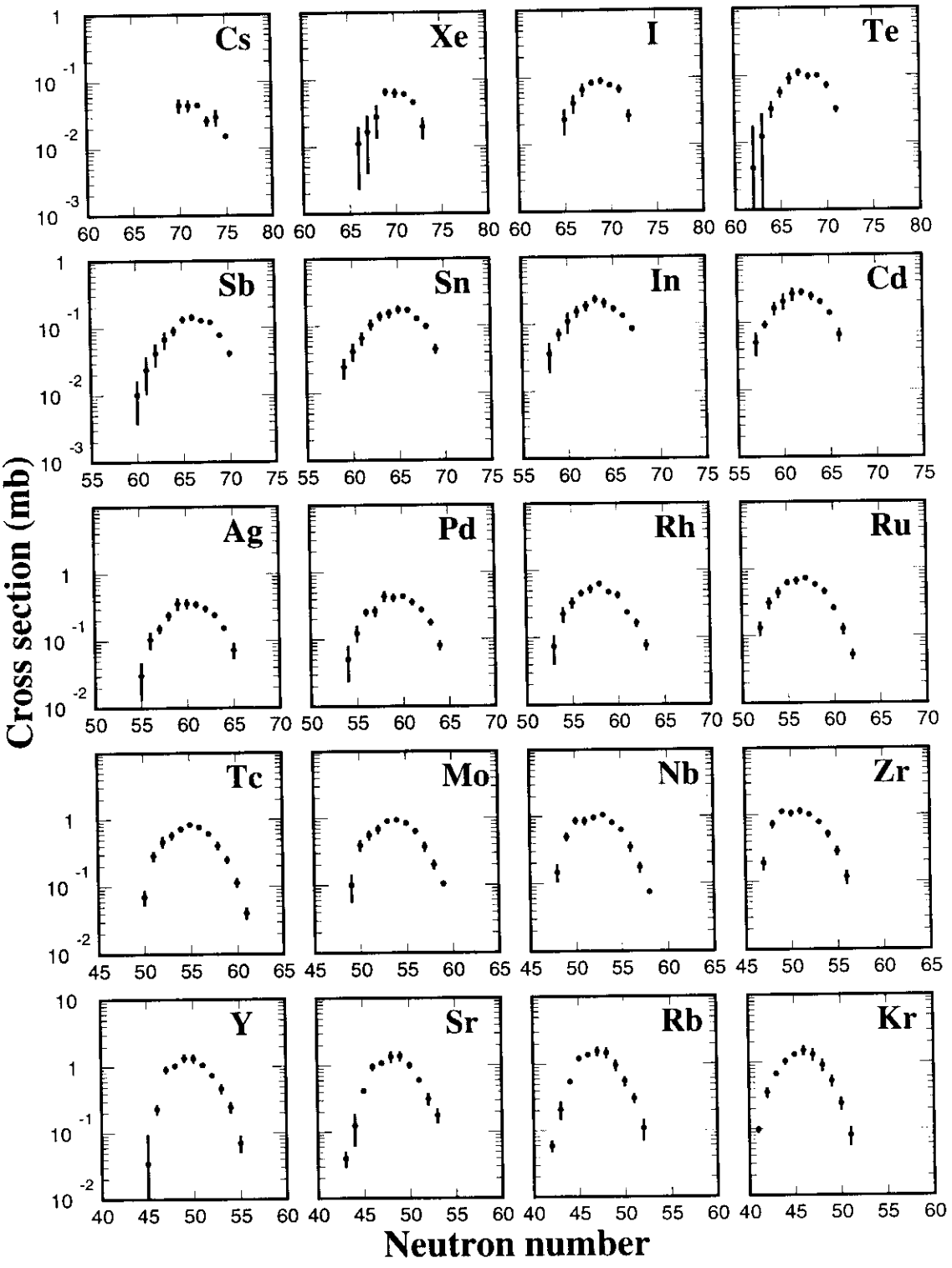

Fig. 6. *Isotopic production cross sections of fission residues from the reaction* $^{197}Au(800\ A\ MeV) + p$. *The error bars correspond to the statistical uncertainty.*

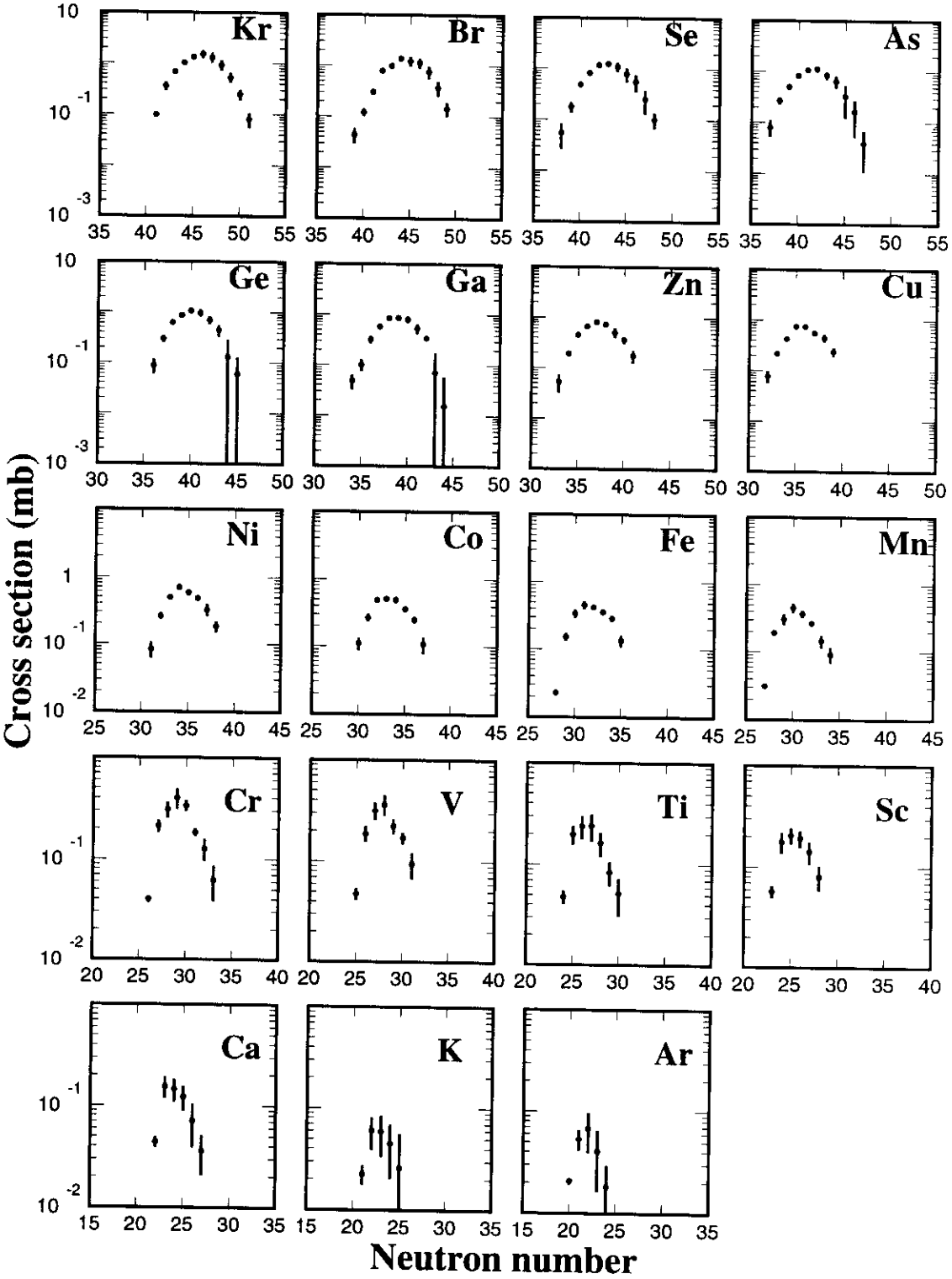

Fig. 7. *Isotopic production cross sections of fission residues from the reaction* $^{197}Au(800\ A\ MeV) + p$. *The error bars correspond to the statistical uncertainty.*

Table 1
Comparison of the production cross sections of some shielded isotopes obtained by Michel et al., (σ_{mi}) for the reaction p(800 MeV)+^{197}Au [8] and Kaufman et al.(σ_{kau}) for the reaction p(1000 MeV)+^{197}Au [9], using gamma-spectroscopic methods, with the corresponding results of the present work (σ_{GSI}). The errors of the cross sections obtained in this work correspond to the statistical uncertainty. An additional systematic error of 15% should be considered.

Isotope	σ_{mi}(mb)	σ_{kau}(mb)	σ_{GSI}(mb)
^{102}Rh	0.80±0.13		0.53±0.08
^{96}Tc	0.78±0.06	0.72±0.09	0.58±0.08
^{88}Y	2.45±0.19		1.36±0.20
^{86}Rb	2.41±0.37		0.96±0.18
^{84}Rb	2.01±0.16	1.44±0.25	1.54±0.25
^{82}Br	0.93±0.17		0.76±0.21
^{74}As	1.37±0.11	1.38±0.13	1.07±0.10
^{60}Co	0.75±0.09		0.51±0.05
^{58}Co	0.96±0.09	0.41±0.06	0.27±0.03
^{54}Mn	0.39±0.05	0.44±0.04	0.31±0.06
^{46}Sc	0.17±0.02	0.38±0.05	0.21±0.04

4 Results and discussion.

4.1 Comparison with existing data.

The scarce existing data where isotopic production cross sections have been determined in proton on ^{197}Au induced fission reactions at energies around 800 MeV were obtained by using gamma-spectroscopic methods [8,9]. This technique allows to determine individual production cross sections only for isotopes shielded by a long-lived or stable precursor in the β-decay chain.

In table 1, we compare the production cross sections of some shielded fission residues measured by Michel et al. [8] for the reaction p(800 MeV) + ^{197}Au (σ_{mi}) and Kaufman et al. [9] for the reaction p(1000 MeV) + ^{197}Au (σ_{kau}), using gamma-spectroscopic methods, with the ones obtained in this work (σ_{GSI}). As can be seen, in general the spectroscopic cross sections are at least 40% larger than the ones obtained in the present work. Similar discrepancies are observed between both spectroscopic measurements for ^{84}Rb, ^{58}Co and ^{46}Sc that probably could not be explained from the difference in energy of the proton beam.

Table 2
Total fission cross sections for proton on ^{197}Au reactions at energies around 800 MeV. (*) In this work the total fission cross section is determined from the sum of the measured isotopic production cross sections. This value underestimates the true total fission cross section since our isotopic distributions are truncated at 0.05 mb on the average.

Reaction	σ_f^{tot}(mb)	reference
p(660 MeV) + ^{197}Au	75±9	[29]
p(600 MeV) + ^{197}Au	76±15	[30]
p(1000 MeV) + ^{197}Au	71±7	[31]
p(1000 MeV) + ^{197}Au	72.4±3.4	[32]
p(1000 MeV) + ^{197}Au	94±19	[30]
p(1000 MeV) + ^{197}Au	66±7	[33]
p(1000 MeV) + ^{197}Au	69±9	[34]
^{197}Au(800 A MeV) + p	65±10	this work*

In order to conclude about these discrepancies, we also compare our total fission cross section (σ_f^{tot} = (65±10) mb) with the values obtained in previous dedicated experiments. A compilation of the results obtained in these experiments is shown in table 2. Additionally, a systematic evaluation of all previously measured proton-induced total fission cross sections was done in Ref. [35]. An overall systematics was obtained giving a total fission cross section for the reaction p(800 MeV)+^{197}Au of σ_f^{tot} = 74.2 mb.

Our experimental value coincides with the systematics within the error bars. Indeed, our measured total fission cross section is expected to be slightly smaller than the real one since very low cross sections in the wings of the isotopic distributions could not be determined. If we assume that the isotopic distributions are truncated at 0.05 mb on the average (see Figs. 6 and 7), a rough estimate of this missing part, distributed over many isotopes, yields a value of 8 mb. This brings our value up to about 73 mb which is very close to the systematic value of Ref. [35]. This agreement proves the accuracy of the measured production yields and the corrections applied to obtain cross sections.

The smooth behavior of the isotopic distributions obtained in the present work (see figures 6 and 7) demonstrates that the observed discrepancies between these data and the ones obtained by gamma spectroscopy can not be due to any anomaly in the evaluation of the cross section of specific isotopes.

Additional information can be obtained from the work of Andronenko et al. [10]. These authors determined the total fission cross section together with

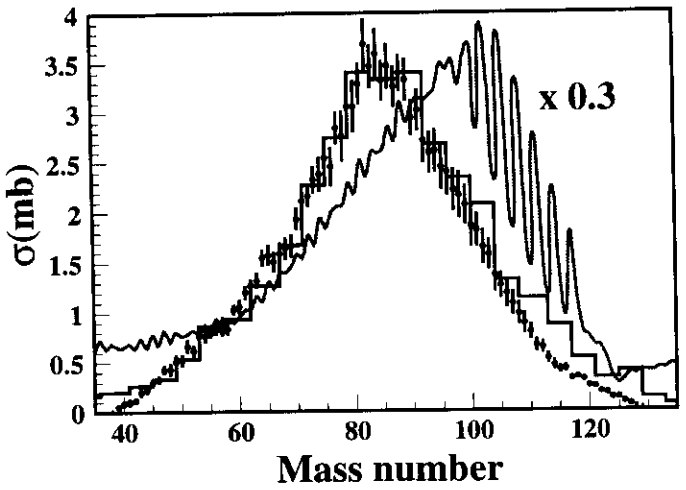

Fig. 8. *Mass distribution of the fission residues produced in the reaction ^{197}Au+p (solid points) compared with the mass distribution of fission residues from reference [10] for the reaction p(1000 MeV)+^{197}Au (histogram). The error bars of the experimental data correspond to the statistical uncertainty. The experimental values are also compared with the predictions obtained with a semi-empirical parameterization [36] of the isotope production cross sections in spallation reactions (solid line). Note that the empirical predictions have been scaled by a factor of 0.3.*

the mass distribution of fission fragments produced in the reaction p(1000 MeV)+^{197}Au using a two arms time-of-flight spectrometer. The total fission cross section obtained in this work amounts to $\sigma_f^{tot} = (71\pm7)$ mb, which is in good agreement with our measured value. The mass distribution of fission residues is reported in figure 8 (histogram) and compared with the one obtained in the present work (solid points). As can be seen, not only the total fission cross section but also the mass distribution of the fission fragments is in excellent agreement. The slightly broader mass distribution at 1000 MeV (7%) may be explained in terms of the difference in excitation energy induced by the protons at 800 MeV and at 1000 MeV.

4.2 Comparison with semi-empirical parameterizations.

In Fig. 8, we compare the measured mass distribution of fission residues with the predictions obtained with the semi-empirical parameterizations of Silberberg et al. [36] to describe the residue production in spallation reactions. As can be seen, the calculated mass distribution is far from any agreement with the present data or those obtained in reference [10]. Neither the shape nor the absolute value of the measured distributions are described with this kind of parameterization. Large discrepancies are also obtained when we compare the isotopic production cross sections with the predicted ones. Differences larger

Table 3
Parameters characterizing the mass and charge distribution and the kinematics of fission residues in ^{197}Au-on-proton collisions at 800 A MeV obtained in this work. In order to consider the bias in the measured distributions due to the lower limit of the measurements, the mean values and the standard deviations were obtained from Gaussian fits of a restricted range of the distributions. The considered range of the mass, charge and neutron number distributions were A=60-110, Z=25-48 and N=34-60 respectively.

σ_f^{tot}(mb)	$\langle$A$\rangle$	$\langle$Z$\rangle$	$\langle$N$\rangle$	σ_A	σ_Z	σ_N	$\langle E_K \rangle$ (MeV)
65±10	85	37.5	47.5	14.8	6.5	8.5	121

than one order of magnitude in the production cross sections are observed for many of the isotopes.

These huge discrepancies can be understood as a consequence of the lack of experimental information concerning the mass and charge distribution of fission residues produced in spallation-fission reactions. Indeed, also theoretical models are not able to fully reproduce the isotope production in spallation reactions, as shown in references [6,7]. The present data provide a new benchmark to improve not only semi-empirical parameterizations but also more elaborated theoretical models.

4.3 Mass and charge distribution.

In table 3, we report the main parameters describing the mass and charge distribution of fission residues obtained in the present work. The difference in mass observed between half the value of the primary projectile ^{197}Au and the mean value of the measured mass distribution of fission residues is an indication of the excitation energy induced in the collision manifested in terms of particle emission.

The mass distribution of fission residues of pre-actinides is known to be symmetric. In reference [37], the authors have systematically determined the evolution of the width of the mass distributions of pre-actinide nuclei as a function of its fissility at low excitation energy (E≈10 MeV) from experimental data. In the region of fissility covered by the possible fissioning nuclei produced in the reaction ^{197}Au(800 A MeV)+p ($Z^2/A \approx 30-32$) the measured width of the mass distributions of fission residues amounts to σ_A ≈8-9. The value obtained in this work (σ_A=14.8) is almost a factor of two larger than the ones obtained in low-energy fission. Two effects contribute to the broadening of the mass distribution in the fission induced by 800 MeV protons in ^{197}Au: First, the excitation energies of the fissioning nuclei are presumably much higher and, secondly, several fissioning nuclei might contribute to the observed distribu-

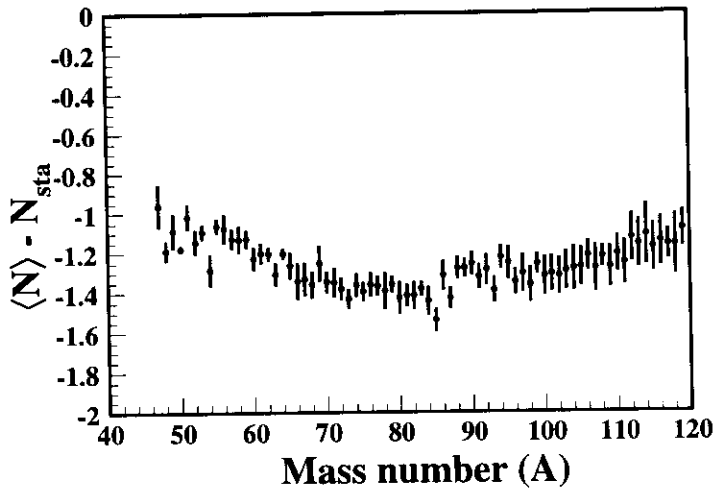

Fig. 9. *Difference between the measured mean neutron number for isobaric distributions* $\langle N \rangle$ *and the neutron number of the stable isotopes* N_{sta} *versus the mass number. The error bars represent the standard deviations of the isobaric distributions.*

tions. A more detailed analysis of these reaction aspects will be carried out on the basis of elaborate model calculations in a forthcoming publication [7]. Here, we restrict ourselves to a phenomenological discussion of the measured distributions.

The region of the chart of the nuclides populated by the measured fission residues can be characterized by the mean value of the isobaric distributions and their standard deviations. In Fig. 9 we report the difference between the mean value of the isobaric distributions and the neutron number of the β-stable isotopes as a function of the mass number. The β-stable isotopes were defined according to Ref. [38] by the following expression:

$$Z_{sta} = \frac{A}{1.89 + 0.0155 \cdot A^{2/3}} \tag{10}$$

As can be seen, the mean neutron number of the measured fission residues is very close to that of the stable isotopes. Therefore, the fission residues produced in the reaction ^{197}Au(800 A MeV)+p are distributed along the β-stability valley. Consequently, great part of the fission cross section corresponds to stable isotopes. Two important conclusions can be drawn from this result: First, the cumulative yields obtained by gamma-spectroscopic techniques miss an important fraction of the fission yields. Secondly, the fission of pre-actinides is not an optimum process for the production of exotic nuclei.

In Fig. 10, we report the standard deviation of the isotopic distribution as a

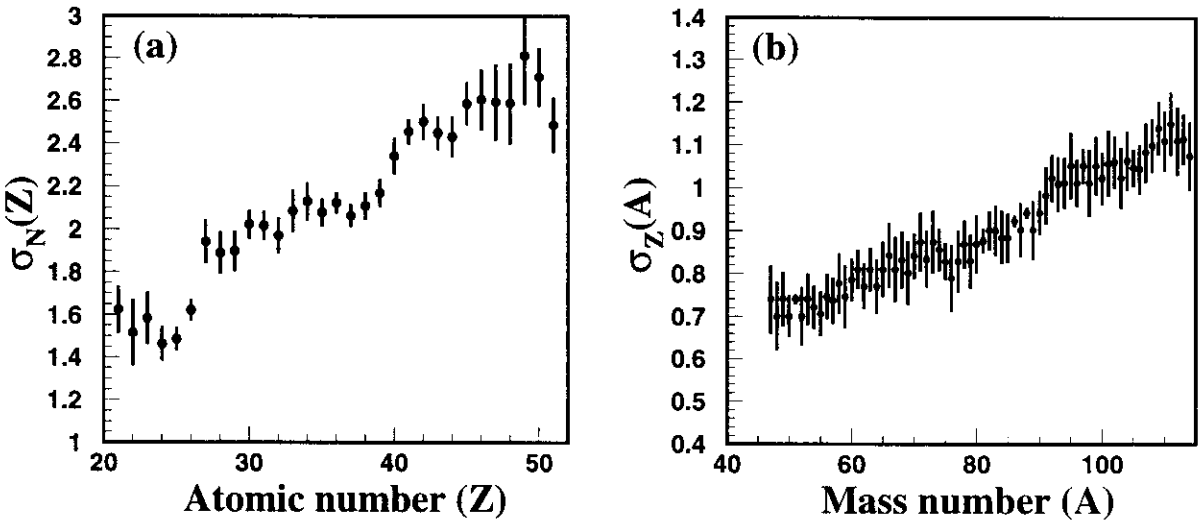

Fig. 10. *(a) Standard deviation of the isotopic distribution $\sigma_N(Z)$ as a function of the atomic number. (b) Standard deviation of the isobaric-charge distribution $\sigma_Z(A)$ as a function of the mass number. The error bars represent the uncertainty due to the fitting procedure.*

function of the atomic number (a), and the standard deviation of the isobaric-charge distribution as a function of the mass number (b). In both pictures, we observe a broadening of the isotopic and isobaric distribution of fission residues with their atomic number or mass. This effect could be explained in terms of the energy sharing between both fission fragments. A partition of the energy according to the mass would explain the observed evolution of the standard deviations of the distributions of fission residues. A similar behavior was obtained in the fission of highly excited fragments from collisions of 750 A MeV ^{238}U on lead [15]. In contrast, the isobaric charge distribution of fission residues produced in low-energy fission for the same reaction does not show any dependence of its standard deviation according to the mass number [14].

The mean neutron number of the isobaric distributions $\langle N \rangle$ (Fig. 9) together with the standard deviations of the isotopic $\sigma_N(Z)$ and the isobaric $\sigma_Z(A)$ distributions (Fig. 10) gives a full description of the mass and charge distribution of the fission residues produced in the reaction ^{197}Au(800 A MeV)+p assuming a Gaussian-like distribution of the isotopic distributions. These values will help to improve semi-empirical parameterizations describing the isotope production in spallation reactions as the one presented in reference [36].

4.4 Kinetic energies.

The kinetic energies of the fission residues can be determined from the isotopic identification and the precise determination of the velocity by the magnetic-

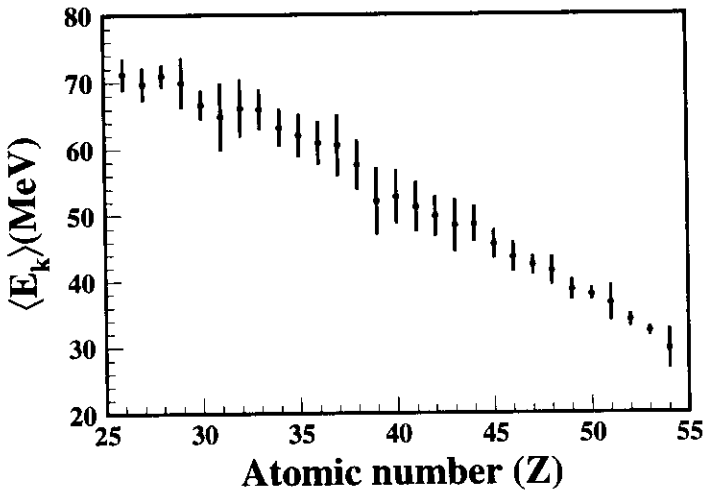

Fig. 11. *Mean kinetic energies of the measured fission residues as a function of their atomic number. The error bars represent the standard deviation of the kinetic-energy distribution of the isotopes with the same atomic number.*

rigidity measurement at the intermediate image plane of the spectrometer according to the expression:

$$\beta\gamma = \frac{e}{c}\frac{(B_1\rho_1)\cdot Z}{m_o \cdot A} \tag{11}$$

where β is the relativistic velocity and $\gamma = (1-\beta^2)^{-1/2}$, e is the elementary electric charge and m_o is the atomic mass unit. The index 1 refers to the first half of the FRS.

In Fig. 11, we represent the mean kinetic energy of the fission residues as a function of their atomic number. The error bars represent the standard deviation of the kinetic-energy distribution of the isotopes with the same atomic number. The measured kinetic energy follows the expected dependence with the atomic number due to the correlation between the mass and the velocity of the fission residues produced by momentum conservation in the fission process. These values can be compared with the systematics of fission-fragment total kinetic energy established by Viola et al. [39]. If we assume that the fissioning system has a mass and an atomic number twice the mean mass and atomic number of the measured fission residues distributions ($A_{CN} \approx 170$, $Z_{CN} \approx 75$) the expected total kinetic energy according to the systematics is $\langle E_k \rangle_{Vio} \approx$ 128 MeV. The systematics is confirmed by the measured mean kinetic energy assuming a symmetric fission $\langle E_k \rangle \approx 121$ MeV.

5 Conclusion and outlook.

The isotopic production cross sections of fission residues in a spallation-fission reaction from a fissioning pre-actinide have been measured for the first time. The use of the inverse kinematics together with the in-flight separator FRS at GSI seems to be the optimal technique to identify all the reaction residues in mass and atomic number and to determine their production cross sections with high accuracy.

The comparison of the measured data in the present work with others obtained for the same reaction gives different results. In general, we observe large discrepancies with the production cross sections of specific isotopes shielded against β-decay obtained with gamma-spectroscopic methods. In contrast, remarkably good agreement is obtained with the mass distribution of fission residues measured with time-of-flight techniques and with the total fission cross sections obtained in dedicated experiments.

The present data have also been compared with semi-empirical descriptions of the isotope production in spallation reactions. This comparison shows severe discrepancies which demonstrate that the semi-empirical parameterization can not be extrapolated to regions where experimental data do not exist.

Several conclusions were also drawn from the qualitative analysis of the charge and mass distributions of the fission residues produced in the reaction studied. The large width of the mass distribution of the fission fragments suggests that the fission process takes place at rather high excitation energies. A similar conclusion is obtained from the evolution of the standard deviations of the isotopic distributions as a function of the atomic number and the isobaric-charge distributions as a function of the mass number.

The analysis of the isotopic distribution of the fission residues also reveals that the produced fission residues are mainly distributed along the β-stability valley. Two important conclusions can be drawn from this result. The cumulative yields obtained with gamma-spectroscopic methods can not be representative of the mass distribution of the fission residues of pre-actinides because a large fraction of the cross section corresponds to stable isotopes. This result also indicates that the fission of pre-actinides is not an optimum process to produced exotic nuclei.

The experimental technique used in this work also allowed to determine the kinetic energies of the fission residues. The measured values coincide with the systematics established by Viola et al. This information is also relevant not only for a better understanding of the fission process but also to investigate the behavior of spallation targets irradiated with intense proton fluxes.

Finally, we state that the present data constitute a solid basis for future benchmarks of theoretical models describing the spallation process.

The authors are indebted to J. Taieb and J. Pereira for providing the calculations for secondary reactions in the target and transmission corrections, respectively, and to K.H. Behr, A. Brünle and K. Burkhard for their technical support to this experiment. This work was partially supported by the European Union under contract ERBFMGECT950083 and by the "Secretaría Xeral de Investigación e Desenvolvemento de la Xunta de Galicia" under contract number PGIDT99PXI20602A.

References

[1] The European Spallation Source Study, vol III, The ESS Technical Study, report ESS-96-53-M, 1996

[2] C.D. Bowman, E.D. Arthur, P.W. Lisowski, G.P. Lawrence, R.J. Jensen, J.L. Anderson, B. Blind, M. Cappiello, J.W. Davidson, T.R. England, L.N. Engel, R.C. Haight, H.G. Hughes III, J.R. Ireland, R.A. Krakowski, R.J. LaBauve, B.C. Letellier, R.T. Perry, G.J. Russel, K.P. Staudhammer, G. Versamis, W.B. Wilson, Nucl. Instr. and Methods A 320 (1992) 336

[3] W.F. Henning, Nucl. Instr. and Methods B 126 (1997) 1

[4] H. Reeves, W.A. Fowler, F. Hoyle, Nature 226 (1970) 727

[5] R. Michel, P. Nagel, International Codes and Model Intercomparison for intermediate energy activation yields. NSC/DOC(97)-1, NEA/P&T No 14

[6] F. Rejmund, B. Mustapha, J. Benlliure, T. Enqvist, L. Tassan-Got, K.-H. Schmidt, P. Armbruster, M. Bernas, A. Boudard , J.P. Dufour, S. Leray, R. Legrain, C. Stéphan, J. Taieb, C. Volant, to be submitted to Nucl. Phys. A

[7] J. Benlliure, P. Armbruster, M. Bernas, A. Boudard, J.P. Dufour, T. Enqvist, F. Rejmund, R. Legrain, S. Leray, B. Mustapha, K.-H. Schmidt, C. Stéphan, L. Tassan-Got, C. Volant, in preparation

[8] R. Michel, R. Bodemann, H. Busemann, R. Daunke, M. Gloris, H.-J. Lange, B. Klug, A. Krins, I. Leya, M. Lupke, S. Neumann, H. Reinhardt, M. Schnatz-Buttgen, U. Herpers, Th. Schiekel, F. Sudbrock, B. Holmqvist, H. Conde, P. Malmborg, M. Suter, B. Dittrich-Hannen, P.-W. Kubik, H.-A. Synal, D. Filges, Nucl. Instr. and Methods B 129 (1997) 153

[9] S.B. Kaufman, E.P. Steinberg, Phys. Rev. C 22 (1980) 167

[10] L.N. Andronenko, A.A. Kotov, M.M. Nesterov, V.F. Petrov, N.A. Tarasov, L.A. Vaishnene, Z. Phys. A 318 (1984) 97

[11] Yu. A. Chestnov, A.V. Kravtsov, B. Yu. Sokolovsii, G.E. Solyakin, Sov. J. Nucl. Phys. 45 (1) 1987

[12] J.R. Cummings, W.R. Binns, T.L. Garrad, M.H. Israel, J. Klarmann, E.C. Stone, C.J. Waddington, Phys. Rev. C 42 (1990) 2508 and Phys. Rev. C 42 (1990) 2530

[13] P. Armbruster, M. Bernas, S. Czajkowski, H. Geissel, T. Aumann, Ph. Dessagne, C. Donzaud, E. Hanelt, A. Heinz, M. Hesse, C. Kozhuharov, Ch. Miehe, G. Münzenberg, M. Pfützner, K.-H. Schmidt, W. Schwab, C. Stephan, K. Sümmerer, L. Tassan-Got, B. Voss, Z. Phys. A 355 (1996) 191

[14] C. Donzaud, S. Czajkowski, P. Armbruster, M. Bernas, C. Böckstiegel, , Ph. Dessagne, H. Geissel, E. Hanelt, A. Heinz, C. Kozhuharov, Ch. Miehé, G. Münzenberg, M. Pfützner, W. Schwab, C. Stéphan, K. Sümmerer, L. Tassan-Got, B. Voss, Eur. Phys. J. A 1 (1998) 407

[15] W. Schwab, M. Bernas, P. Armbruster, C. Böckstiegel, S. Czajkowski, Ph. Dessagne, C. Donzaud, H. Geissel, E. Hanelt, A. Heinz, C. Kozhuharov, Ch. Miehé, G. Münzenberg, M. Pfützner, C. Stéphan, K. Sümmerer, L. Tassan-Got, B. Boss, Eur. Phys. J. A 2 (1998) 179

[16] T. Enqvist, J. Benlliure, F. Farget, K.-H. Schmidt, P. Armbruster, M. Bernas, L. Tassan-Got, A. Boudard, R. Legrain, C. Volant, C. Böckstiegel, M. de Jong, J.P. Dufour, Nucl. Phys. A 658 (1999) 47

[17] M. Bernas, S. Czajkowski, P. Armbruster, Ph. Dessagne, C. Donzaud, H-R. Faust, E. Hanelt, A. Heinz, C. Kozhuharov, Ch. Miehé, G. Münzenberg, M. Pfützner, C. Röhl, K.-H. Schmidt, W. Schwab, C. Stéphan, K. Sümmerer, L. Tassan-Got, B. Voss, Phys. Lett. B 331 (1994) 19 and Phys. Lett. B 415 (1997) 111

[18] H. Geissel, P. Armbruster, K.-H. Behr, A. Brünle, K.-H. Bukhard, M. Chen, H. Folger, B. Franczak, H. Keller, O. Klepper, B. Langenbeck, F. Nickel, E. Pfeng, M. Pfützner, E. Roeckl, K. Rykaczewski, I. Schall, D. Schardt, C. Scheidenberger, K.-H. Schmidt, A. Schröter, T. Schwab, K. Sümmerer, M. Weber, G. Münzenberg, T. Brohm, H.-G. Clerc, M. Fauerbach, J.-J. Gaimard, A. Grewe, E. Hanelt, B. Knödler, M. Steiner, B. Voss, J. Weckenmann, C. Ziegler, A. Magel, H. Wollnik, J.P. Dufour, Y. Fujita, D.J. Vieira, B. Sherrill, Nucl. Instr. and Methods B 70 (1992) 286

[19] M. Pfützner, H. Geissel, G. Münzenberg, F. Nickel, C. Scheidenberger, K.-H. Schmidt, K. Sümmerer, T. Brohm, B. Voss, H. Bichsel, Nucl. Instr. and Methods B 86 (1994) 213

[20] B. Voss, T. Brohm, H.-G. Clerc, A. Grewe, E. Hanelt, A. Heinz, M. de Jong, A. Junghans, W. Morawek, C. Röhl, S. Steinhäuser, C. Ziegler, K.-H. Schmidt, K.-H. Behr, H. Geissel, G. Münzenberg, F. Nickel, C. Scheidenberger, K. Sümmerer, A. Magel, M. Pfützner, Nucl. Instr. and Methods A 364 (1995) 150

[21] K.-H. Schmidt, E. Hanelt, H. Geissel, G. Münzenberg, J.P. Dufour, Nucl. Instr. and Methods A 260 (1987) 287

[22] N. Iwasa, H. Geissel, G. Münzenberg, C. Scheidenberger, Th. Swab, J. Wollnik Nucl. Instr. and Methods B 126 (1997) 284

[23] Transport, D.C. Carey, K.L. Brown, F. Rothacker, SLAC-R-95-462

[24] J. Benlliure, J. Pereira, K.-H. Schmidt, to be submitted to Nucl. Instr. and Methods

[25] C.J. Benesh, B.C. Cook, J.P. Vary, Phys. Rev. C 40 (1989) 1198

[26] S. Kox, C. Perrin, J. Arvieux, R. Bertholet, J.F. Bruandet, M. Buenerd, R. Cherkaoui, A.J. Cole, Y. El-Masri, N. Longequeue, J. Menet, F. Merchez, J.B. Viano, Phys. Rev. C 35 (1987) 1678

[27] T. Brohm, Ph.D. Thesis, TH Darmstadt (1994)

[28] A.R. Junghans, H.-G. Clerc, A. Grewe, M. de Jong, J. Müller, K.-H. Schmidt, Nucl. Instr. and Methods A 370 (1996) 312

[29] Konshin et al., Yadernaya Fiz. 2 (1965) 682

[30] J. Hudis, S. Katcoff, Phys. Rev. C 13 (1976) 1961

[31] L.A. Vaishnene, L.N. Andronenko, G.G. Kovshevny, A.A. Koto, G.E. Solyakin, Z. Phys. A 302 (1981) 143

[32] B.A. Bochagov, V.S. Bychenkov, V.D. Dmitriev, S.P. Mal'tsev, A.I. Obukhov, N.A. Perfilov, V.A. Udod, O.E. Shigaev, Sov. J. Nucl. Phys. 2 (1978) 28

[33] J. Hudis, S. Katcoff, Phys. Rev. 180 (1969) 1122

[34] W.R. Binns, T. L. Garrard, M. H. Israel, M. P. Kertzmann, J. Klarmann, E. C. Stone, C. J. Waddington, Phys. Rev. C 36 (1987) 1870

[35] A.V. Prokofiev, accepted for publication in Nucl. Instr. and Methods A

[36] R. Silberberg, C.H. Tsao, A.F. Barghouty, Astr. Phys. J. 501 (1998) 911

[37] S.I. Mulgin, K.-H. Schmidt, A. Grewe, S.V. Zhdanov, Nucl. Phys. A 640 (1998) 375

[38] P. Marmier, E. Sheldon, "Physics of Nuclei and particles", Academic Press 1969, pag. 36

[39] V.E. Viola, K. Kwiatowski, M. Walker, Phys. Rev. C 31 (1985) 1550